

Parametric Uncertainty Identification and Model Reduction for Robust H_2 Synthesis for Track-Following in Dual-Stage Hard Disk Drives

Richard Conway, Sarah Felix and Roberto Horowitz

Abstract—This paper presents a systematic, semi-automated method for identifying parameters and parametric uncertainty for a set of dual-stage hard disk drives. A modal analysis technique is selected to extract parameters from a batch of frequency response data. In order to avoid redundancy in modal parameters, a method of data fusion is incorporated into the modal analysis to find common parameters for multiple frequency response functions. Next, a model truncation methodology is presented as an alternative way to eliminate redundant parameters from a multiple-input-multiple-output system model. In both model reduction methods, optimization algorithms are employed to minimize the error associated with the reduced order model. Finally, convex optimization and singular value decomposition are employed to obtain a low-order, minimally conservative approximation of uncertain parameters. The result is a reduced order state space model with parametric uncertainty to be used in robust H_2 control synthesis for a track-following hard disk drive servo.

I. INTRODUCTION

Increasing areal data densities in hard disk drives continue to motivate the development of high performance servo schemes for track-following control. Among the emerging configurations are dual-stage servos which incorporate a smaller-scale actuator onto the disk drive suspension in addition to the voice coil motor (VCM) [1], [2]. It has also been shown that the use of optimal robust control synthesis techniques along with realistic disturbance models and modeling uncertainties results in dual-stage controllers with superior tracking performance [3].

A significant challenge in the implementation of control design techniques such as robust H_2 synthesis is the identification of model parameters and uncertainties. Since robust H_2 synthesis optimizes over all the worst case combinations of the uncertain parameters, the computation time increases dramatically as the number of uncertain parameters increases. Thus, obtaining a description of the plant uncertainty with a minimal number of parameters is essential for posing a computationally feasible control design problem. This can be achieved through proper selection and identification of the model form, appropriate model reduction, and a reduced-order approximation of the set of uncertain parameters. The following presents systematic methods for each of these phases of system identification, originating from a set of experimental frequency response functions (FRFs). The

This work was supported in part by National Science Foundation grant CMS-0428917, the Information Storage Industry Consortium and the Computer Mechanics Laboratory at UC Berkeley

R. Conway, S. Felix, and R. Horowitz are with the Department of Mechanical Engineering, University of California, Berkeley rconway345@berkeley.edu, sarfelix@me.berkeley.edu, horowitz@me.berkeley.edu

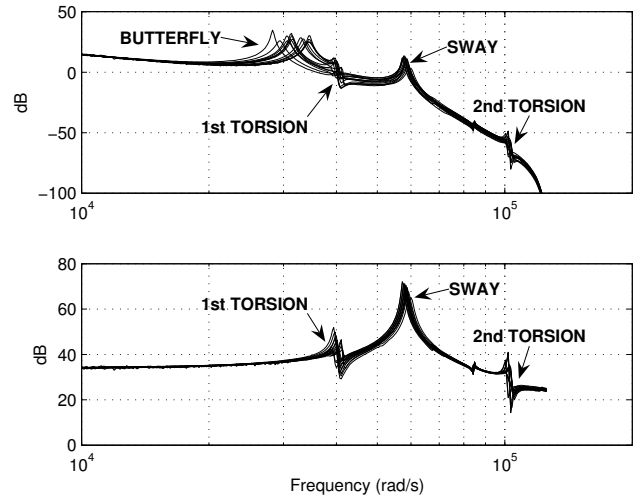


Fig. 1. Experimental frequency response data from 15 plants. Top: VCM to off-track displacement, bottom: PZT to off-track displacement.

methods are presented in the context of a practical example application.

II. MODEL IDENTIFICATION

A. Model Form

Fig. 1 shows the experimental frequency response data for a batch of 15 dual-input, single-output hard disk drive plants obtained from [4]. The secondary input is piezoelectric (PZT) actuation of the suspension. Several distinct resonance modes are apparent in the data. It is therefore appropriate to represent the transfer function between each input-output pair, $G_{ij}(s)$, as a summation of N modes, as follows:

$$G_{ij}(s) = \sum_{k=1}^N \left[\frac{b_0}{s^2 + \eta\omega_n s + \omega_n^2} \right]_{ij,k} \quad (1)$$

This form requires only three parameters per mode: natural frequency, ω_n , damping coefficient, η , and modal constant, b_0 . These modal parameters relate to insight about physical plant variations, which motivates the uncertainty analysis described in Section IV.

B. Modal Parameter Identification

Parameters for each mode in the summation form are identified readily using single degree of freedom (SDOF) modal analysis. A SDOF model is based on the assumption that near a resonance frequency, the frequency response of a system is

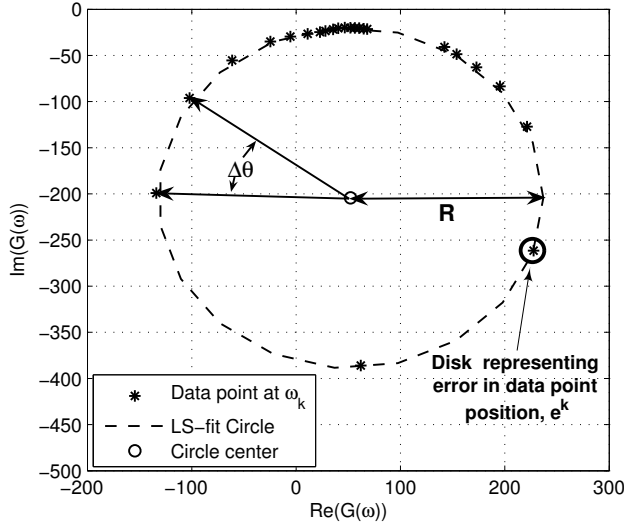


Fig. 2. A least squares-based circle fit to the frequency response data points around the 1st torsion mode of the PZT response of one plant.

dominated by the dynamics of that resonance mode, and the contribution from other modes is a constant. This assumption is typically valid for disk drive structures [5], but should be verified by checking that the data points around each peak form a distinct ellipse when plotted in the Nyquist plane. In particular, when the FRF represents a displacement response and when the damping near each resonant frequency can be approximated by structural damping, as in

$$\bar{G}_{ij}(s) = \sum_{k=1}^N \left[\frac{b_0}{s^2 + (\eta\omega_n^2/\omega)s + \omega_n^2} \right]_{ij,k}, \quad (2)$$

the ellipse is an exact circle [6]. This property is exploited for parameter identification, since ω_n , η , and b_0 can be extracted from the geometry of the circle, and a circle can be easily fit using a least squares algorithm. The equations for computing the modal parameters are derived from the complex function $G_{ij}(j\omega)$ as in [6]. Fig. 2 illustrates a circle of data points in the Nyquist plane. The least squares fit determines the center of the circle and its radius, R .

The natural frequency, ω_n , is the frequency at which the sweep rate of the data points around the circle, γ , is maximum, with γ defined by

$$\gamma(\omega^2) = \frac{d\theta}{d(\omega^2)} \approx \frac{\Delta\theta}{\Delta(\omega^2)}. \quad (3)$$

The remaining modal parameters are then given by the following equations:

$$\eta = \frac{2}{\omega_n^2 \gamma_{max}} \quad (4)$$

$$b_0 = 2R\omega_n^2\eta. \quad (5)$$

It is clear in Fig. 2 that the resolution of the data points is poor, especially where sweep rate is at its maximum. This leads to significant error in the modal parameter estimates. A solution to this problem is to first fit some nominal curve,

$G_{nom}(s)$, to the experimental data, and then use this curve to pick off points of arbitrary density around the peak of each mode. $G_{nom}(s)$ does not have to be constrained to the form in (1). It only has to provide an analytical transfer function that fits the data well. In some instances, the modal parameters can be extracted directly from $G_{nom}(s)$, but it was found that this is not generally the case and the circle fit method is more robust.

This technique is used to obtain modal parameters from the FRFs for each plant in the batch. Fig. 3 shows a model fit to data points using the circle fit method. Five modes are identified in the VCM transfer function and three modes are identified in the PZT transfer function, for a total of sixteen states in the model. Finally, for each plant, the identified transfer functions are combined to form a multiple-input-multiple-output (MIMO) state space realization such that

$$G(s) = C(sI - A)^{-1}B. \quad (6)$$

Since it is possible that some modes may be considered negligible, a priori knowledge is required from the designer about which modes are to be identified. The designer would thus make a tradeoff between model order and the importance of the modes in tracking controller performance.

III. DATA FUSION METHOD FOR REDUCING PLANT ORDER

A. Obtaining Common Parameters

It is evident in Figs. 1 and 3 that there are several modes that appear in both sets of FRFs, meaning both actuators excite some of the same modes in the structure. This leads to nearly redundant sets of eigenvalue pairs in the A matrix of the state space system, with slight differences being the result of error in measurements and parameter estimation. One way to avoid this redundancy is to simultaneously fit the data from the FRFs of all input-output pairs in order to extract common values for natural frequency and damping. Such *Multi-fit* or *global* fitting techniques are sometimes used in modal analysis to combine data, improving parameter estimates in the presence of uncertainty [7]. Here, a method is proposed that combines the data at an intermediate step of the circle fitting algorithm. Further, the data is combined in a statistically meaningful manner by a weighted average based on variances. Note that another user decision is required to specify which modes are redundant.

As shown in (3)-(5), natural frequency and damping estimates both depend on γ_{max} . Further, common modes that occur in different FRFs will theoretically have the same $\gamma(\omega^2)$. As such, merging experimental data to get common values of $\gamma(\omega^2)$ is an efficient way to obtain common estimates of both natural frequency and damping. Fig. 4 shows the sweep rate for a torsion mode in both the VCM response and the PZT response of a single plant. In the real data, there are differences in $\Delta\theta$ between the two data sets due to measurement and curve fitting error. Therefore, it makes sense to combine the sweep rate data using a weighted average based on the variance of each set of data. This

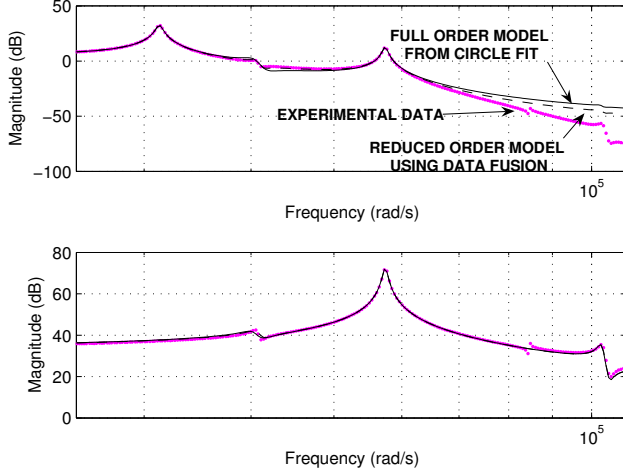


Fig. 3. Model from circle fit method with and without data fusion compared to data points for one plant (showing only magnitude plots).

weighted average is statistically justified using the principle of maximum likelihood, as in [8].

First, variance is characterized based on the error of the nominal curve fit, $G_{nom}(s)$. Because a least squares-based algorithm was used to compute $G_{nom}(s)$, it is expected that the real and imaginary components of the error are Gaussian with zero mean and a covariance proportional to the identity matrix. In the Nyquist plane, this means that the components of the error in any rotated set of coordinates are also Gaussian and the second order statistics are preserved. Thus, the curve-fit error can algebraically related to the sweep rate as follows. Let e^k be the error between data point k and the value of $G_{nom}(j\omega_k)$ at the corresponding frequency. Then consider the tangential component of e^k relative to the Nyquist circle mapped from $G_{nom}(j\omega)$, denoted by e_t^k , and let ν be the variance of e_t^k . Since e_t^k is much smaller than R , the error in θ , e_θ^k , can be approximated by

$$e_\theta^k \approx \sin e_\theta^k = \frac{e_t^k}{R} \quad (7)$$

Then, the variance of e_θ can be computed by

$$\nu_\theta = E[(e_\theta^k)^2] = \frac{\nu}{R^2} \quad (8)$$

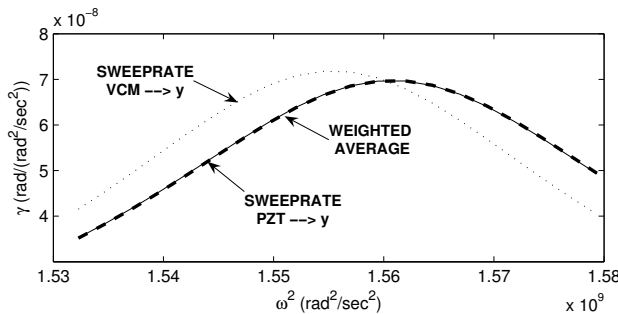


Fig. 4. Angular sweep rate of FRF data points around the Nyquist plane circle for the 1st torsion mode.

Since two data points are needed to calculate $\Delta\theta$, the error propagates using root-sum-squares, assuming the component errors are Gaussian [8]. This assumption is valid since θ is related to e_t by a factor of R . The variance of $\Delta\theta$, $\nu_{\Delta\theta}$, is then

$$\nu_{\Delta\theta} = \frac{\sqrt{2}\nu}{R^2}. \quad (9)$$

Finally, the estimate, $\widehat{\Delta\theta}$, is computed from a weighted average using the inverse of the variances of i data sets:

$$\widehat{\Delta\theta} = \frac{\sum_i \Delta\theta / \nu_{\Delta\theta i}}{\sum_i 1 / \nu_{\Delta\theta i}} = \frac{\sum_i \Delta\theta / \nu_i}{\sum_i 1 / \nu_i}. \quad (10)$$

Fig. 4 shows $\gamma(\omega^2)$ computed using $\widehat{\Delta\theta}$. Note that the new curve is heavily weighted toward the curve associated with the PZT response. The reason for this is that the PZT response has a much larger magnitude resulting in a larger circle, and therefore more reliable estimates of $\Delta\theta$.

Once common estimates are obtained for natural frequency and damping coefficient, separate modal constants can be extracted from the circle radii of the individual data sets, as in (5). Fig. 3 shows the the resulting model fit to the data. The new model is very similar to the model obtained without data fusion, but it has only ten states instead sixteen states. Note that while it is possible that the model obtained using data fusion may fit the experimental data better than without data fusion, there is no guarantee that the error will decrease.

B. Pointwise Optimization of the State Space Model

To address the issue of minimizing model fit error, this section presents a technique to improve a state space realization by comparing its frequency response to a set of frequency response data. In particular the B and C matrices will be optimized to improve the fit of the model to the experimental data. It is assumed that the A matrix adequately captures the system eigenvalues after parameter estimation. This is valid for three reasons. First, natural frequency tends to be easy to estimate accurately. Second, while the damping coefficient is typically more difficult to estimate, it has been observed that closed loop controllers are relatively insensitive to error in the damping coefficient [9]. Finally, error in modal constants that arises from cross-coupling of modes due to violations of the SDOF assumption does not affect the A matrix.

For the state space realization (6) and the experimental frequency response data (of which we have measurements at frequencies $\omega_1 < \dots < \omega_L$), respectively define $G_{lk}(j\omega)$ and $F_{lk}(j\omega)$ to be the SISO frequency responses between the k^{th} input and the l^{th} output. Let $W_{lk}(j\omega)$ be a weighting function between the k^{th} input and the l^{th} output. Then with the definitions

$$H_{lk}(j\omega) = W_{lk}(j\omega) [G_{lk}(j\omega) - F_{lk}(j\omega)] \quad (11)$$

$$2\alpha_i^2 = \begin{cases} \omega_2 - \omega_1 & i = 1 \\ \omega_{i+1} - \omega_{i-1} & 1 < i < L \\ \omega_L - \omega_{L-1} & i = L \end{cases} \quad (12)$$

$$J_{mrr}^p = \sum_{l=1}^m \sum_{k=1}^n \sum_{i=1}^L |\alpha_i H_{lk}(j\omega_i)|^2 \quad (13)$$

the optimization to be approximately solved is

$$\min_{B,C} J_{mr}^p. \quad (14)$$

These values of α_i were chosen so that, by the trapezoidal rule,

$$\sum_{i=1}^L \alpha_i^2 |H_{lk}(j\omega_i)|^2 \approx \int_{\omega_1}^{\omega_L} |H_{lk}(j\omega)|^2 d\omega. \quad (15)$$

Thus the cost function can be interpreted as

$$J_{mr}^p \approx 2\pi \sum_{l=1}^m \sum_{k=1}^n \|W_o H_{lk}(s)\|_2^2 \quad (16)$$

where W_o is the frequency window function for $[\omega_1, \omega_L]$. As a side note, although the trapezoidal rule was chosen for convenience here, any integration rule could be chosen to select the values of α_i .

Fixing the value of C and defining

$$\Phi_{ik} = \begin{bmatrix} W_{1k}(j\omega_i)c_1 \\ \vdots \\ W_{mk}(j\omega_i)c_m \end{bmatrix} (j\omega_i I - A)^{-1} \quad (17)$$

$$\psi_{ik} = \begin{bmatrix} W_{1k}(j\omega_i)F_{1k}(j\omega_i) \\ \vdots \\ W_{mk}(j\omega_i)F_{mk}(j\omega_i) \end{bmatrix} \quad (18)$$

$$\Phi_k = [\Phi_{1k}^T \quad \cdots \quad \Phi_{Lk}^T]^T \quad (19)$$

$$\psi_k = [\psi_{1k}^T \quad \cdots \quad \psi_{Lk}^T]^T \quad (20)$$

where c_i is the i^{th} row of C gives, after a bit of simplification,

$$\min_{b_1, \dots, b_n} J_{mr}^p = \sum_{k=1}^n \min_{b_k} \left\| \begin{bmatrix} \mathcal{R}\{\Phi_k\} \\ \mathcal{I}\{\Phi_k\} \end{bmatrix} b_k - \begin{bmatrix} \mathcal{R}\{\psi_k\} \\ \mathcal{I}\{\psi_k\} \end{bmatrix} \right\|^2 \quad (21)$$

where b_i is the i^{th} column of B and \mathcal{R} and \mathcal{I} respectively denote the real and imaginary parts of a matrix. Since the norm in this expression is the Euclidean norm, the optimal B can be found using least squares.

Now note that when a system is transposed, the C matrix becomes the transpose of the B matrix. Since transposing $G(j\omega)$ and flipping the indices on $F_{lk}(j\omega)$ and $W_{lk}(j\omega)$ does not change the problem, the problem of finding the optimal C while keeping A and B fixed is equivalent to finding the transpose of the optimal B matrix for the transposed systems.

Although B and C cannot be optimized simultaneously using this methodology, they can be optimized one at a time in an alternating, iterative fashion until the model reduction cost, J_{mr}^p , converges. Because this optimization is formulated as a least squares problem, the solution converges quickly and reliably. In addition, in this framework, it is easy to impose equality constraints on certain parameters. In this way, entries in the original state space realization which are zero will remain unchanged, avoiding an increase in the number of uncertain parameters.

Fig. 5 shows pointwise optimization applied to a reduced order model that was obtained using the data fusion algorithm described in the previous section. A weighting function

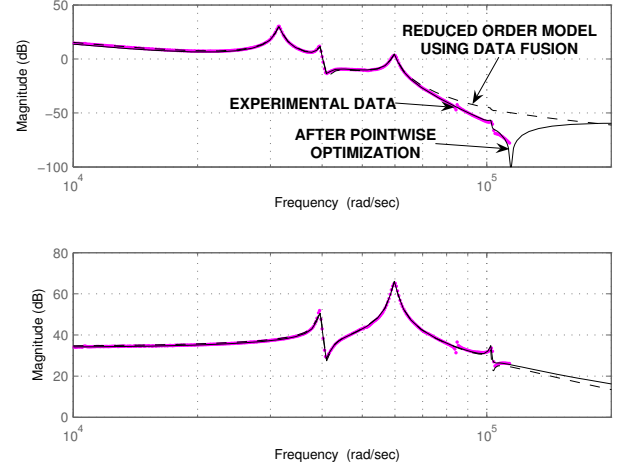


Fig. 5. Reduced order model optimized with respect to experimental data.

defined by the inverse of the magnitude of the experimental response was applied to normalize the cost at all frequencies. The optimized model fits the data points well. However, the optimum fit is guaranteed only for the frequencies at which data is available. In this example, the pointwise optimization results in additional zeros that distort the model outside of the frequency range of the data. It is important to note here that continuous time models are being fit to discrete time sampled data. The experimental frequency response exhibits distortion as the frequency approaches the Nyquist frequency corresponding to the sampling rate, or $1.26 \cdot 10^5 \text{ rad/s}$. Thus the optimized model introduces artificial dynamics while trying to match the distortion. It is expected that modifying the optimization algorithm for discrete time systems will result in a better model, even outside of the frequency range of the data.

IV. MODEL REDUCTION VIA OPTIMIZED TRUNCATION

The previous section discusses a method of directly consolidating experimental data to obtain common parameters. An alternative means of reducing the model order is to eliminate redundant eigenvalues in the MIMO state space realization using model reduction techniques. As a first step in this process, the order of the model is reduced using balanced model truncation [10]. Because the repeated pairs of modes are weakly observable, balanced model truncation effectively eliminates the redundant eigenvalues in the A matrix. It is assumed here that the designer specifies either the number of redundant modes, or the threshold for truncation based on the Hankel singular values. Although a balanced model truncation is fast to compute and results in small additive H_∞ norm error [10], it is not optimal in any sense. In the case of the dual stage system, since the redundant modes are not necessarily weakly controllable, information is lost in the B and C matrices, resulting in significant error shown in Fig. 6. Notice that despite the error, the modes appear at the

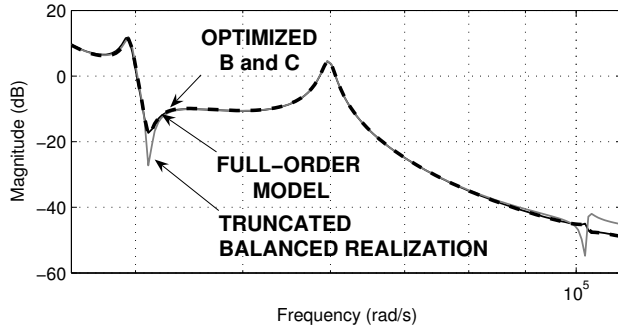


Fig. 6. Bode magnitude plot of the displacement output response to VCM input showing full-order and reduced-order models.

correct frequencies, indicating that the correct eigenvalues were preserved.

An additional optimization step improves the accuracy of the reduced-order system. This additional step is based on H_2 model reduction, which is currently a problem which can only be approximately solved using nonlinear, non-convex optimization [11]. The H_2 norm is used here because it corresponds to least squares in the frequency domain. As an alternative to finding a globally optimal reduced-order model, a method will be presented to refine the B and C matrices of the reduced-order model via H_2 model optimizations with closed-form solutions.

Let the state space realization of the reduced order model by given by

$$\hat{G}(s) = \hat{C} (sI - \hat{A})^{-1} \hat{B}. \quad (22)$$

For the full order plant and the reduced order plant, respectively define $G_{ij}(s)$ and $\hat{G}_{ij}(s)$ to be the single-input-single-output (SISO) transfer functions between the j^{th} input and the i^{th} output. Let $\bar{W}_{ij}(s)$ be a stable, causal SISO weighting function between the j^{th} input and the i^{th} output. Then with the definitions

$$\bar{H}_{ij}(s) = \bar{W}_{ij}(s) [G_{ij}(s) - \hat{G}_{ij}(s)] \quad (23)$$

$$J_{mr} = \sum_{i=1}^m \sum_{j=1}^n \|\bar{H}_{ij}(s)\|_2^2 \quad (24)$$

the optimization to be approximately solved is

$$\min_{\hat{B}, \hat{C}} J_{mr}. \quad (25)$$

Let $\bar{W}_{ij}(s)$ have the realization

$$\bar{W}_{ij}(s) \sim \left[\begin{array}{c|c} A_{ij}^W & B_{ij}^W \\ \hline C_{ij}^W & D_{ij}^W \end{array} \right]. \quad (26)$$

Defining b_i to be the i^{th} column of B , \hat{b}_i to be the i^{th} column to \hat{B} , c_i to be the i^{th} row of C and \hat{c}_i to be the i^{th} row of

\hat{C} , $\bar{H}_{ij}(s)$ can be realized as

$$\bar{H}_{ij}(s) \sim \left[\begin{array}{ccc|c} A_{ij}^W & B_{ij}^W c_i & -B_{ij}^W \hat{c}_i & 0 \\ 0 & A & 0 & b_j \\ 0 & 0 & \hat{A} & \hat{b}_j \\ \hline C_{ij}^W & D_{ij}^W c_i & -D_{ij}^W \hat{c}_i & 0 \end{array} \right] \quad (27)$$

$$= \left[\begin{array}{c|c} A_{ij}^H & B_{ij}^H \\ \hline C_{ij}^H & D_{ij}^H \end{array} \right].$$

Note that A_{ij}^H and C_{ij}^H are not functions of \hat{B} . Thus, with the assumption that \hat{A} and \hat{C} are known, it is possible to solve for the observability gramian, Q_{ij} , of $\bar{H}_{ij}(s)$ by using the following Lyapunov equation:

$$(A_{ij}^H)^T Q_{ij} + Q_{ij} A_{ij}^H + (C_{ij}^H)^T C_{ij}^H = 0. \quad (28)$$

The H_2 norm of $\bar{H}_{ij}(s)$ is then given by

$$\|\bar{H}_{ij}(s)\|_2^2 = (B_{ij}^H)^T Q_{ij} B_{ij}^H, \quad (29)$$

which is quadratic in \hat{b}_j . The minimization with respect to \hat{B} can then be carried out by expressing (24) in terms of the \hat{b}_j vectors using (29) and setting the relevant derivatives equal to 0. The optimal values of the \hat{b}_j vectors are given by

$$\hat{b}_j^o = - (Q_j^{33})^{-1} (Q_j^{23})^T b_j \quad (30)$$

where

$$\left[\begin{array}{ccc} Q_j^{11} & Q_j^{12} & Q_j^{13} \\ * & Q_j^{22} & Q_j^{23} \\ * & * & Q_j^{33} \end{array} \right] = \sum_{i=1}^m Q_{ij}. \quad (31)$$

As with the pointwise algorithm described in Section III, finding the optimal \hat{C} can be found by transposing the state space systems and weights. Although \hat{B} and \hat{C} cannot be optimized simultaneously using this methodology, they can be optimized one at a time in an alternating, iterative fashion until J_{mr} converges.

Fig. 6 shows the Bode magnitude plot of the optimized reduced order model. Note that the optimized reduced order model is much closer to the full order model at frequencies close to the natural frequencies of the plant.

V. UNCERTAINTY APPROXIMATION

A. Minimally Conservative Uncertainty Characterization

After a suitable reduced order model is obtained for each plant, the uncertainty in each parameter (e.g. ω_n) can be characterized. The vector of uncertain parameters, q , is represented as

$$q = \bar{q} + M\delta, \quad \|\delta\|_\infty \leq 1 \quad (32)$$

where \bar{q} represents the vector of nominal parameter values, δ is a vector of unknown real perturbations, and M is a square scaling matrix. Note that the j^{th} reduced order model contains a value of the i^{th} parameter, which will be denoted x_{ij} . Thus, for the j^{th} reduced order plant, the measurement vector is defined as

$$v_j = [x_{1j} \quad \cdots \quad x_{mj}]^T. \quad (33)$$

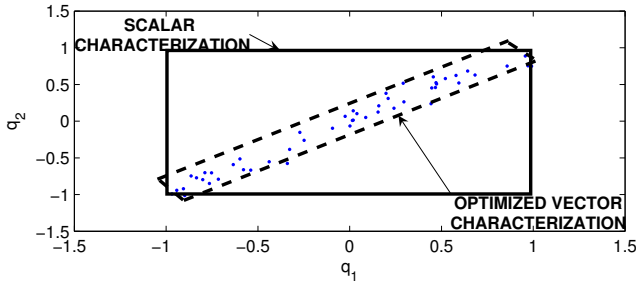


Fig. 7. Illustrative set of measurements for two uncertain parameters.

It can now be seen that the characterization of the uncertain parameters requires the choice M and \bar{q} such that each measurement vector can be described by a proper choice of δ .

Since the objective of robust controller design techniques is to design controllers that meet performance and/or robustness criteria for all $\|\delta\|_\infty \leq 1$, it is crucial to make M “small” so that the uncertainty description is minimally conservative. To quantify the size of M , the volume spanned by all feasible values of $M\delta$ will be used. Since minimizing the volume spanned by the set of feasible values of $M\delta$ is equivalent to minimizing the determinant of M , the problem to be solved is

$$\begin{aligned} \min_{M, \bar{q}} \det M \text{ subject to:} \\ \forall j \exists \delta^j : \|\delta^j\|_\infty \leq 1, \bar{q} + M\delta^j = v_j. \end{aligned} \quad (34)$$

The following are two approaches to solving this problem.

1) *Scalar Characterization*: If the uncertain parameters are assumed to have no coupling, i.e. M is a diagonal matrix, then the i^{th} uncertain parameter, q_i , is represented as

$$q_i = \bar{q}_i + m_i \delta_i, \quad |\delta_i| \leq 1. \quad (35)$$

The problem (34) can then be decoupled into a set of equivalent scalar optimizations which have closed form solutions given by

$$\begin{bmatrix} \bar{q}_i^* \\ m_i^* \end{bmatrix} = \frac{1}{2} \begin{bmatrix} 1 & 1 \\ 1 & -1 \end{bmatrix} \begin{bmatrix} \max\{x_{i1}, \dots, x_{in}\} \\ \min\{x_{i1}, \dots, x_{in}\} \end{bmatrix} \quad (36)$$

The solid box in Fig. 7 illustrates uncertainty characterized in this way for a hypothetical set of two uncertain parameters. Since the parameter measurements range from -1 to 1 , it is trivial to see that for this case, the scalar characterization is given by $\bar{q}_1^* = \bar{q}_2^* = 0$, $m_1^* = m_2^* = 1$. However, much of the box $[-1, 1] \times [-1, 1]$ does not contain any measurements of the parameter, i.e. it is very conservative.

2) *Vectorial Characterization*: To find an less conservative uncertainty characterization than the scalar characterization, it is necessary to exploit the correlation in parameter variation. For example, Fig. 7 illustrates a rotated parallelogram which has less area than the original box, but still encompasses all of the measurements.

Based on this observation, the constraint that M is diagonal will be relaxed to M being symmetric and, without loss of generality, positive semi-definite. The problem (34)

can be equivalently formulated with a linearizing change of variables as

$$\begin{aligned} \max_{Z \succeq 0, p} (\det Z)^{1/r} \text{ subject to:} \\ \|Zv_j - p\|_\infty \leq 1, \quad j = 1, \dots, n \end{aligned} \quad (37)$$

where r is the smallest integer such that $2^r \geq m$. This problem can be represented as a convex semi-definite program (SDP) using YALMIP [12] and solved using SDP solvers such as SeDuMi [13]. In the case when the optimal Z is finite, any SDP solver is guaranteed to find the global minimum in polynomial time. Because the scalar characterization is a special case of this one, this optimization is guaranteed to give better results. Once the optimization has been solved for Z^* and p^* , the corresponding optimal values of M and \bar{q} are recovered by

$$\begin{aligned} M^* &= (Z^*)^{-1} \\ \bar{q}^* &= M^* p^*. \end{aligned} \quad (38)$$

B. Dimensionality Reduction

It can be observed in Fig. 1 that the natural frequency in several modes increases as the associated damping increases, revealing correlation in the model parameter variation. In many physical systems, it is likely that similar coupling exists between parameter measurements such that they can be well-approximated using a reduced-order space. For instance, in Fig. 7, the measurements could be approximated to reasonable accuracy by projecting them onto a line. When using control design methodologies such as robust H_2 synthesis [14] in which the amount of computation required to design a controller increases drastically as the the number of uncertain parameters increases, it is crucial to exploit this coupling and approximate the uncertainty in a system using a small number of parameters.

To begin, define the vector of uncertain parameters as q' and its measurement vectors as y_j . In this framework, a cost function that quantifies how well a k^{th} order subspace approximates the actual data is given by

$$J_k = \sqrt{\sum_{j=1}^n \|y_j - \hat{y}_j\|^2} \quad (39)$$

where \hat{y}_j is the value of y_j after being translated and then projected onto a k^{th} order subspace. The problem of finding the optimal translation and a basis for the optimal k^{th} order subspace under this cost function has a solution which is easy to compute using singular value decomposition (SVD). The optimal translation, \bar{y} is given by the mean of the measurement vectors. Defining $w_j = y_j - \bar{y}$ and performing the SVD

$$[w_1 \quad \dots \quad w_n] = \sum_{i=1}^p \sigma_i (u_i v_i^T) \quad (40)$$

gives a value for $U_k = [u_1 \quad \dots \quad u_k]$, whose columns form the basis of the optimal subspace. The corresponding optimal

value of the cost function is

$$J_k^o = \sqrt{\sum_{i=k+1}^p \sigma_i^2}. \quad (41)$$

With this, the parameters which describe the location in the k^{th} order subspace and the approximation of original uncertain parameter vector are given respectively by

$$q'' = U_k^T (q' - \bar{y}) \quad (42)$$

$$\hat{q}' = U_k q'' + \bar{y}. \quad (43)$$

C. Methodology for Uncertainty Approximation

With the tools for uncertainty characterization and dimensionality reduction in place, it is possible to construct the following semi-automated methodology for uncertainty approximation in a system.

1) *Initial Characterization*: The vector of uncertain parameters, q , is first characterized using the scalar characterization, which gives values of \bar{q} and M . The vectorial characterization is not used here because at this stage, the optimal Z in (37) for this set of uncertain parameters is often not finite.

2) *Dimensionality Reduction*: To nominalize the importance of each uncertain parameter, q' is taken to be δ . The measurements of q' are given by

$$y_j = M^{-1} (v_j - \bar{q}). \quad (44)$$

The designer must now make a decision on how many parameters will be kept. Since there is a closed form solution for the optimal cost as a function of the dimension of the reduced order space (41), a plot of this could aid the designer in this decision. Once this is done, dimensionality reduction gives values of \bar{y} and U_k . This step optimally finds a reduced order space which approximates the uncertainty in the system.

3) *Final Characterization*: The vector of uncertain parameters in the new coordinates is now taken to be $q'' = U_k^T (q' - \bar{y})$, which has the measurement vectors

$$v_j'' = U_k^T (y_j - \bar{y}) \quad (45)$$

Because of the dimensionality reduction, it can be shown that there does not exist a singular scaling matrix for q'' that satisfies the required properties. Thus, the optimal Z in (37) must be finite, and the vectorial characterization can be used to find values of \bar{q}'' and M'' so that $q'' = \bar{q}'' + M'' \delta''$. This step finds the best characterization of the reduced uncertain parameters subject to M being symmetric.

Substitution then gives the approximation of the parameter vector, \hat{q} , by

$$\begin{aligned} \hat{q} &= \bar{q} + M [U_k q'' + \bar{y}] \\ &= (\bar{q} + M\bar{y} + MU_k \bar{q}'') + MU_k M'' \delta''. \end{aligned} \quad (46)$$

This characterization of the parametric uncertainty in the system is optimal in the sense that it minimizes the cost of the approximation, J_k , and also is a minimally conservative characterization with respect to q'' .

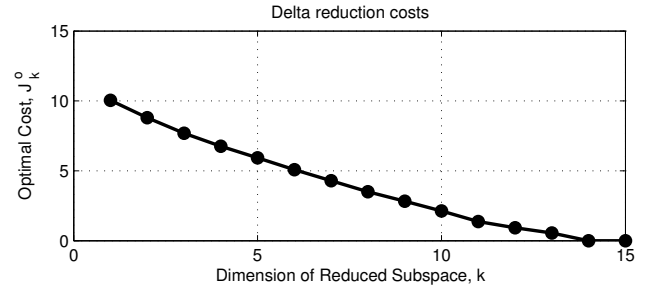


Fig. 8. Perturbation approximation cost vs. dimension of reduced subspace.

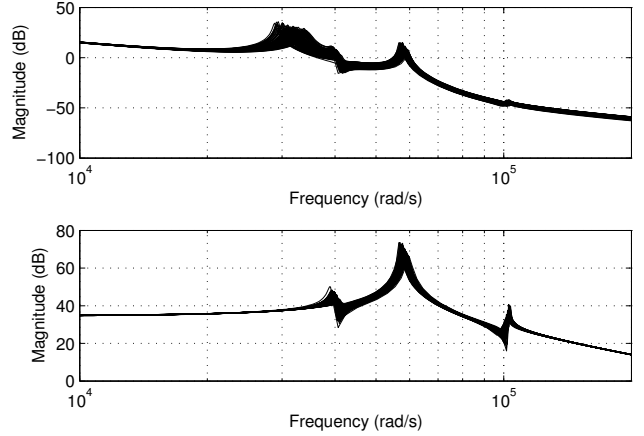


Fig. 9. Bode plots of 100 random samples of the uncertain model characterized by 3 uncertain parameters.

Fig. 8 shows the cost of approximating the parametric uncertainty vs. the dimension of the reduced order space. The obvious part of the design tradeoff is that keeping more uncertain parameters increases the accuracy of the uncertainty description at the cost of increasing the computation time required to design a controller. However, there is also another, more subtle, aspect of the design tradeoff. Previous ad hoc model identification had shown that three uncertain parameters could capture the spread of the parameter values to reasonable accuracy [4]. Fig. 9 shows the Bode magnitude plot of 100 random samples of the final characterization of the uncertain system with three uncertain parameters. Compare this with Fig. 10, which shows the final characterization when all uncertain parameters are kept. Although keeping all of the parameters ensures that all plant variations shown in Fig. 1 are exactly captured by the uncertainty description, it clearly results in a more conservative uncertainty description than the model with only three uncertain parameters. Thus increasing the number of uncertain parameters has the additional cost of increasing the conservatism of the uncertainty description.

VI. CONCLUSIONS AND FUTURE WORK

This paper described algorithms for parameter identification, model reduction, and uncertainty characterization for a set of hard disk drives. The algorithms are based on

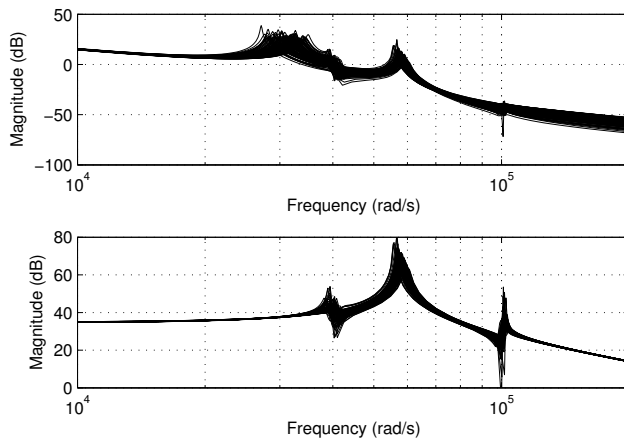


Fig. 10. Bode plots of 100 random samples of the uncertain model characterized by the 14 uncertain parameters.

optimizing meaningful cost functions to effectively manage model order and complexity. Parameter extraction was achieved using a standard SDOF modal analysis technique. Order reduction of the MIMO model was addressed either by simultaneous fitting of multiple experimental data sets, or by model truncation. In both cases, a suitable optimization algorithm was developed to minimize error associated with the reduced order model. Finally, convex optimization and SVD were employed to approximate the uncertain parameters by a smaller, less conservative set of uncertain parameters. The result is an uncertain state space model of manageable size to be used in robust H_2 controller synthesis.

The overall algorithm is semi-automated, requiring some decisions from the control designer. Specifically, it is necessary to select which modes to identify, recognize common modes, and decide how many uncertain parameters to retain. However, these decisions are intuitive and require finite iterations. E.g., the need for extensive trial and error to select parameter and uncertainty values from among infinite possibilities has been eliminated.

The algorithms developed in this paper dealt with continuous time models. As was demonstrated with the pointwise model optimization, this can be problematic when attempting to model a system from sampled data. Future work will modify all algorithms to handle discrete time models.

When characterizing uncertainty, it was assumed that the parameter values identified from the experimental data fully capture the range of possible variations. However, a more realistic approach would account for the stochastic nature of the parameter measurements. One possible method is principal component analysis, which orders parameter coordinates based on the variance in different directions. The solution employs SVD, similar to the deterministic problem presented in Section V. The difference is that the M matrix would be defined by the variances in the direction of the principal components. Future versions of the algorithms presented in this paper will incorporate stochastic methods.

Other future work will involve demonstrating the use the

reduced order model in practical H_2 control synthesis applications and developing user-friendly software to implement the algorithms. In developing user-friendly software, it will be necessary to find effective ways to integrate designer judgement and input into the semi-automated algorithms. Ultimately, the goal is a viable package that will facilitate system identification for uncertain systems, thus expanding the use of robust H_2 control design in the hard disk drive industry and in similar applications.

VII. ACKNOWLEDGMENTS

The authors would like to thank Raymond de Callafon at the University of California, San Diego, for providing the experimental data used in this paper.

REFERENCES

- [1] Y. Li and R. Horowitz, "Design and testing of track following controllers for dual-stage servo systems with pzt-actuated suspensions," *Microsystems Technologies*, vol. 8, pp. 194-205, 2002.
- [2] R. Horowitz, T.L. Chen, K. Oldham and Y. Li, "Design, Fabrication and Control of Micro-Actuators for Dual-Stage Servo Systems in Magnetic Disk Files," *Springer Handbook of Nanotechnology*, ed. B. Bushan, Springer, New York, January 2004.
- [3] X. Huang, R. Nagamune and R. Horowitz, "A Comparison of Multirate Robust Track-Following Control Synthesis Techniques for Dual-Stage and Multi-Sensing Servo Systems in Hard Disk Drives," *IEEE Trans. on Magnetics*, vol.42, no.7, pp. 1896-904, July 2006.
- [4] R. de Callafon, R. Nagamune and R. Horowitz, "Robust Dynamic Modeling and Control of Dual-Stage Actuators," *IEEE Trans. on Magnetics*, vol.42, no.2, pp. 247-54, Feb. 2006.
- [5] K. Oldham, S. Kon, and R. Horowitz, "Fabrication and optimal strain sensor placement in an instrumented disk drive suspension for vibration suppression," *Proceedings of the 2004 American Control Conference IEEE*, vol.2, pp. 1855-61, Piscataway, NJ, USA, 2004.
- [6] D.J. Ewins, *Modal testing: Theory and practice*. J. Wiley & Sons, New York, 1986.
- [7] M. Richardson and D.L. Formenti, "Parameter estimation from frequency response measurements using rational fraction polynomials," *Proc. 1st Int. Modal Analysis Conf.*, pp. 167-182, 1982.
- [8] J.R. Taylor, *An Introduction to Error Analysis*. University Science Books, Mill Valley, CA, USA, 1982.
- [9] J. Choi, R. Nagamune and R. Horowitz, "Synthesis of Multiple Robust Controllers for Parametric Uncertain LTI Systems," *Proceedings of the 2006 American Control Conference*, Minneapolis, MN, IEEE, pp. 3629-3636, Jun. 14-16, 2006. Also to appear in the *International Journal of Adaptive Control and Signal Processing*.
- [10] K. Zhou and J. Doyle, *Essentials of Robust Control*. Prentice Hall, Upper Saddle River, New Jersey, USA, 1998.
- [11] W. Yan and J. Lam, "Approximate approach to H_2 optimal model reduction", *IEEE Transactions on Automatic Control*, vol.44, no.7, pp. 1341-1358, Jul. 1999.
- [12] J. Löfberg, "YALMIP : A toolbox for modeling and optimization in MATLAB," In *Proceedings of the CACSD Conference*, Taipei, Taiwan, 2004. Available from <http://control.ee.ethz.ch/joloef/yalmip.php>.
- [13] J.F. Sturm, "Using SeDuMi 1.02, a matlab toolbox for optimization over symmetric cones," *Optimization Methods and Software*, vol.11-12, pp. 625-653, 1999. Special issue on Interior Point Methods.
- [14] R. Nagamune, X. Huang, and R. Horowitz, "Multi-rate track-following control with robust stability for a dual-stage multi-sensing servo system in HDDs," *Proc. of the Joint 44th IEEE Conference on Decision and Control and European Control Conference ECC 2005*, pp. 3886-3891, Seville, Spain, Dec. 2005.